DETC2018-85450

THREE APPROACHES FOR MANAGING STIFFNESS IN ORIGAMI-INSPIRED MECHANISMS

Alden Yellowhorse

Compliant Mechanisms Laboratory
Department of Mechanical Engineering
Brigham Young University
Provo, Utah 84602
Email: aldenyellowhorse@gmail.com

Larry L. Howell

Professor
Department of Mechanical Engineering
Brigham Young University
Provo, Utah 84602
Email: lhowell@byu.edu

ABSTRACT

Ensuring that deployable mechanisms are sufficiently rigid is a major challenge due to their large size relative to their mass. This paper examines three basic types of stiffener that can be applied to light, origami-inspired structures to manage their stiffness. These stiffeners are modeled analytically to enable prediction and optimization of their behavior. The results obtained from this analysis are compared to results from a finite-element analysis and experimental data. After verifying these models, the advantages and disadvantages of each stiffener type are considered. This comparison will facilitate stiffener selection for future engineering applications.

NOMENCLATURE

- α Panel sector angles
- A Panel area
- a Distance of force in four-point test from outer edge
- B The crease whose angle is used to measure partial actuation in the test prototype
- b Width of a panel cross-section
- C Foam thickness
- c Vertical coordinate of the section centroid
- Δ The area cost
- Δ_r The ratio between the deployed area and the area of one face of a cube of equivalent volume

- δ Ratio between the density of a foam and its constituent material
- d Width of the partially-actuated prototype
- ε_{cd} The strain at the initiation of densification
- E Young's Modulus
- E_f Young's Modulus of the foam core surface
- E_s Young's Modulus of the foam core center material
- F Total force applied to test bending stiffness
- f Parametric parameter h/w
- γ The fold angle at a crease
- H_{max} Maximum fraction of material removed from crease
- H_{min} Minimum fraction of material removed from crease
- h Height of the yielded stiffener
- I Area moment of inertia
- k Effective spring constant
- λ The ratio of E_f/E_s
- L Largest prototype dimension
- μ Fold angle multiplier
- η Ratio between face and core material densities ρ_f/ρ_s for the expanded stiffener
- M The ratio between the current mass and the initial mass
- N Safety factor
- ρ_c Density of the core
- ρ_f Density of the face material
- ρ_s Density of the material in the core
- P Parameter describing the cost of a stiffener size
- p Ratio of b/t

- Q First moment of the area
- a Ratio C/t
- R Ratio of I for the stiffened un-stiffened version
- r Unit-less ratio of w/t
- σ_{el} Constant collapse stress for an elastic foam
- S Maximum acceptable shear stress
- s crease length
- θ The tilt angle of the panel cross-section in a partially-actuated vertex
- T Thickness of the wall of a foam core panel
- t Thickness of a panel cross-section
- V Shear force at a cross-section
- w Total width of a single yielded stiffener unit
- Unitless parameter describing size of a generic stiffener size relative to a specific panel dimension

1 Introduction

The potential of origami to inspire the design of deployable mechanisms has been discussed by various authors in recent years [1–3]. Applications such as spacecraft antennas [4], optical equipment [5] and solar collectors [6] represent just a few of the possible roles that these devices can fill advantageously. However, the design of deployable mechanisms for these applications is a significant challenge. One concern that applies specifically to these large, light-weight structures is their ability to maintain their designed shape under their loads. This designed deployed shape could be specified by a number of factors. For an antenna, the shape would be governed by the signal wavelength it was designed to transmit or receive. The shape of a solar collector or optical array also needs to be closely controlled to achieve their function.

Nevertheless, controlling the shape of the array can be particularly challenging when dealing with origami panels deployed over a large area. Origami-inspired mechanisms often consist of a collection of thin panels connected with hinges that are folded into a small package for transportation. When ready to deploy, these folded mechanisms are generally deployed into a large, relatively flat and thin configuration [7]. While the packing efficiency is high, the resulting deployed configuration is vulnerable to shape distortion because of its low bending stiffness.

In a space application, this distortion could be introduced by a variety of factors, including the manufacturing tolerances and materials used to construct the array [8]. Another important factor is the load placed on the array by reaction wheels used to control the spacecraft and other mechanisms such as cryocoolers [9, 10]. Thermal distortions can also influence the deployed configuration of the structure [11]. These factors make it essential to design deployable structures with enough stiffness to resist applied loads and maintain their desired configuration.

This paper describes three methods of changing the deployable geometry and adjusting the stiffness of a large, origamiinspired deployed structure. Folding methods are used so that the advantages of origami systems are retained and to maintain compatibility with the methods used to construct the origami system. Procedures for assessing the potential change in stiffness produced by this method are examined. One method involves partially folding the entire pattern in order to enhance stiffness. The use of a rib that is yielded into place along a crease is also examined. Finally, the use of panels with expandable, foam cores that increase stiffness is proposed. In all cases, the positioning and proportions of the stiffeners are considered to facilitate the optimal design of these components.

2 Background

Understanding the stiffness of a deployed structure is a fundamental problem that has been investigated by several researchers [12–14]. Tan and Pellegrino [15] extensively studied the properties of a stiffener located at the edge of a flexible dish. Their work investigated specific problems with this stiffener such as flexibility, vibration and stiffness. Research on the use of stiffeners at the hinge of a deployable solar array has also been conducted by Jorgensen et al. [16] Their work focused on the dynamics of the deployment process but still illustrated the use of such stiffeners to obtain specific behavior in their deployable mechanism.

Research performed by Schenk and Guest [17] specifically focused on the modeling of stiffness in textured origami sheets. The difference in the stiffness of these patterns in different modes of deformation was considered to give insight into origami mechanism design. A similar analysis of the stiffness of different modes of deformation was performed by Filipov et al. [18] while specifically examining variations of origami zippers. Their research highlighted the ability of these origami mechanisms to provide both a compliant, deployable mode and a stiff load-bearing mode.

Work has also been performed on characterizing origami tessellations as a meta-material and computing its mechanical characteristics. For example, Cheung et al. [19] discuss the possibility of using cellular origami tessellations to enable the construction of light, strong structures that can retain deployability. Their work discusses both the kinematics and mechanics of the resulting structures and its capacity to resist loads as well as permit motion. Similarly, Wonoto et al. [20] investigate the ability of simple origami tessellations to support their own weight when deployed. They also conduct an optimization of the geometry to meet this structural need.

3 Methods for Managing Pattern Stiffness

When constructing an origami-inspired deployable mechanism, many factors need to be considered before decisions about its design can be made, including the inherent stiffness of the de-

ployed pattern and its complexity. The complexity and usefulness of additional stiffeners would also be a factor. In this section, different methods for managing the stiffness of an origami pattern are discussed and their relative advantages and disadvantages are listed to facilitate their design.

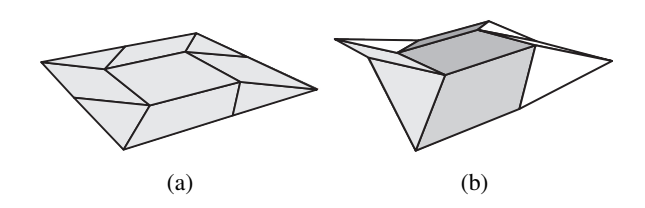


FIGURE 1: (a) A flat pattern and a (b) partially folded version used to enhance the panel stiffness

3.1 Partially Folded Patterns

The first method for managing pattern stiffness is partially folding a pattern as shown in Figure 1. Making this alteration to the pattern can be advantageous because it requires no modification to the device design and so can be implemented at a low cost. However, it may necessitate other changes if the original surface was required to be perfectly flat. Nevertheless, if this partial folding is minimized, any negative side effects may reduce to acceptable levels. To quantify how much folding is necessary to sufficiently increase stiffness, the kinematics of individual origami vertices must be modeled.

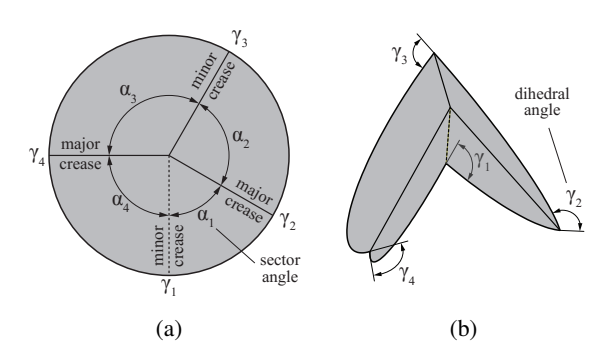


FIGURE 2: (a) A flat vertex and a (b) partially folded version [21]

It has been demonstrated [21] that the fourth-order origami vertex shown in Figure 2a can be modeled using the fold-angle

multiplier

$$\mu = \frac{\sin\left[\frac{1}{2}(\alpha_1 + \alpha_2)\right]}{\sin\left[\frac{1}{2}(\alpha_1 - \alpha_2)\right]} \tag{1}$$

and the relationship between major and minor fold angles

$$\tan\left(\frac{1}{2}\gamma_2\right) = \mu \tan\left(\frac{1}{2}\gamma_1\right) \tag{2}$$

Here, α_1 and α_2 are the sector angles of two panels not divided by the minor crease line, and γ_1 is the dihedral angle between the panel containing α_1 and α_2 . The dihedral angle γ_2 is the angle between the panels containing α_1 and α_2 . The angles γ_1 and γ_2 are defined as zero when the pattern is flat and π when it is fully folded. Opposite dihedral angles are equal, or $\gamma_1 = \gamma_3$ and $\gamma_2 = \gamma_4$.

If the folded angles γ_1 and γ_2 are limited to small angles where $\gamma \le 0.2$ and $\tan x \approx x$ then we have

$$\gamma_2 \approx \mu \gamma_1$$
 (3)

which demonstrates that at small dihedral angles, the major and minor dihedral angles γ_1 and γ_2 are related linearly. More generally, all the dihedral angles in a pattern composed of fourth-order vertices are linearly related. This is important because it permits the characterization of the area moment of inertia of any cross-section perpendicular to the face of the origami model.

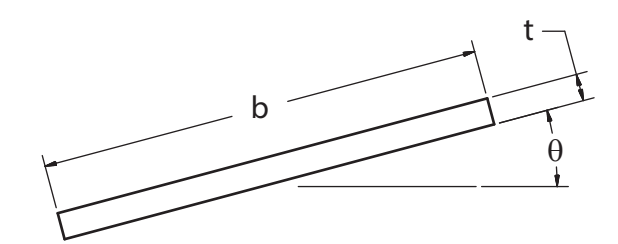


FIGURE 3: The tilted configuration of a panel in a partially folded pattern

If a cut is made using a plane perpendicular to the face of the origami, then the resulting cross-section will be composed of a certain number of connected segments. These segments will be approximately rectangular if the thickness of the panels is much less than its length. If these segments are tilted at an angle θ , then the area moment of inertia of the segment is given by

$$I = \frac{bt}{12} (t^2 \cos^2 \theta + b^2 \sin^2 \theta) \tag{4}$$



FIGURE 4: A concept for a yielded stiffener which is cut from the panel

where b is the length of the segment, t is its thickness and θ is its tilt angle as shown in Figure 3. The tilt angle is zero when the segment is completely horizontal. If we make the substitution b = pt, then we have

$$I = \frac{t^4}{12} p(\cos^2 \theta + p^2 \sin^2 \theta^2)$$
 (5)

where p is the ratio of the width (b) to the thickness (t). If we find the ratio of a tilted segment's area moment of inertia to its inertia when flat, R, we find that this ratio is

$$R = \cos^2 \theta + p^2 \sin^2 \theta \tag{6}$$

This relationship shows that for large values of p (i.e. the segment is very thin relative to its thickness), the increase in inertia is large. The potential gains in I is illustrated by considering that if the maximum tolerated actuation angle is $\theta=0.05$ radians, a width to thickness ratio of twenty (p=20) would double the moment of inertia. If it were forty, the inertia ratio would quintuple.

3.2 Yielded Panel Stiffeners

Another possible mechanism for stiffening a panel is to add a plate that can be yielded at its crease and deployed to enhance stiffness. This concept is shown in Figure 4. Employing this type of stiffener promises some important advantages. First, the stiffener could be stamped out of the material and so would be relatively simple to add to a design. Such a stiffener would also automatically lock into place following deployment. While deployment would be an issue due to the nature of the crease in the stiffener, many options exist for driving the motion [22, 23]. The gains in stiffness will be significant as long as the panels in the deployable are thin.

In this section, we will analyze a yielded stiffener and its ability to enhance the bending stiffness of an origami panel. A diagram of the cross-section of the stiffener in Figure 4 is shown in Figure 5. With the given geometry, it is possible to calculate the centroid of the section with respect to y. If the panels are assumed to be thin, then the centroid for the cross-section in Figure 5 is located at

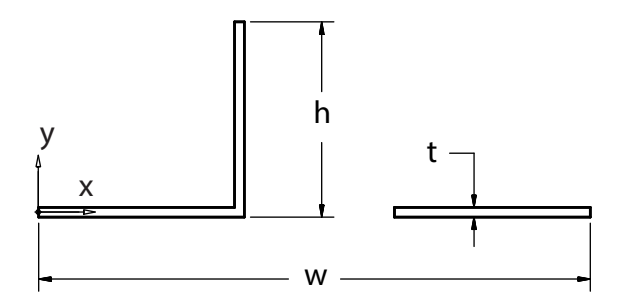


FIGURE 5: The yielded-stiffener cross-section

$$c = \frac{h^2}{2w} \tag{7}$$

respectively where *h*, *t* and *w* are described in Figure 5. Knowing the centroid allows us to calculate the area moment of inertia of the cross-section. This inertia is

$$I = \frac{1}{3}th^3 - \frac{1}{4}\frac{th^4}{w} + \frac{1}{12}t^3w - \frac{1}{12}t^3h$$
 (8)

using the parameters shown in Figure 5. If this inertia is divided by the area moment of inertia of the unmodified panel of width w and thickness t, then we have

$$R = \frac{I}{I_0} = 4r^2f^3 - 3r^2f^4 + 1 - f \tag{9}$$

if we make the parametric substitutions f = h/w and r = w/t. These equations will be accurate until buckling occurs.

3.2.1 Stiffener Crease Perforations Successfully implementing this stiffener type requires some method of deploying it and then locking it into place. One approach for accomplishing this is to perforate the crease about which the stiffener bends. This would provide a predictable bend location as well as a suitable restraining force once the stiffener is fully deployed. An image of the suggested perforations are shown in Figure 6.

A side effect of this perforation is that it predisposes the stiffener to failure in shear at the crease due to bending. The shear at the crease line is given by

$$\tau = \frac{VQ}{It} \tag{10}$$

where Q is derived for the specific geometry shown in Figure 4

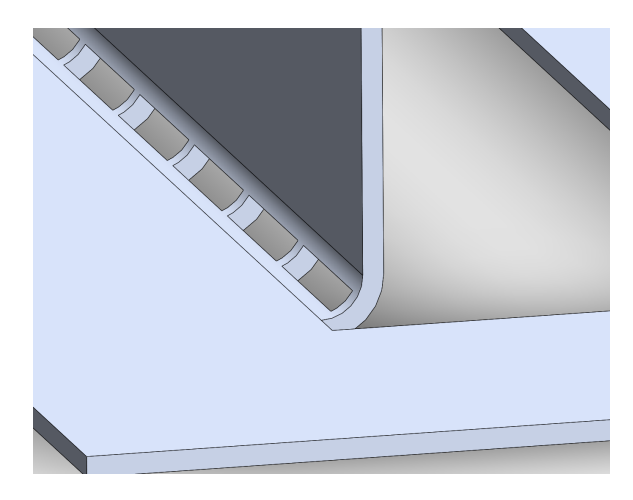


FIGURE 6: Perforations in the crease of the yielded stiffener

and is given by

$$Q = \frac{(w-h)th^2}{2w} \tag{11}$$

This derivation is performed using the method described in [24]. Substituting these values for Q into Equation 10 yields

$$\tau = 6 \frac{h^2 (-w + 2h)V}{t (-4h^3w + 3h^4 - t^2w^2 + t^2wh)}$$
 (12)

$$=6\frac{Vr(-1+2f)f^2}{t^2(-4r^2f^3+3r^2f^4-1+f)}$$
(13)

where V is the shear load applied to the end of the beam. Since this shear stress is the stress felt by the crease if it were fully dense, it must be increased when material is removed. If the maximum tolerable shear stress is S, then the maximum fraction of material that can be removed, H_{max} , is given by

$$H_{max} = 1 - \frac{\tau}{S} \tag{14}$$

3.2.2 Material Removal to Permit Deployment

While H_{max} provides a maximum amount of material that can be removed, the minimum of this quantity should also be determined (H_{min}) . Enough material should be removed so that the stiffener is loaded elastically while the crease is loaded plastically during deployment. If the crease is loaded elastically with a factor of safety N, then the maximum tolerable moment, M_e , is

$$M_e = \frac{\sigma_y s t^2}{6N} \tag{15}$$

where σ_y is the yield strength of the material and s is the crease length. If material is removed from the cross-section and only a fraction of the original cross-sectional area $st(1-H_{min})$ remains, then the plastic moment for the crease is

$$M_p = \frac{(1 - H_{min})st^2}{4}\sigma_y \tag{16}$$

Equating these two moments and solving for H_{min} yields

$$H_{min} = 1 - \frac{2}{3N} \tag{17}$$

Therefore, if N=2 then 2/3 of the crease material should be removed. In this case, the crease will yield plastically while the stiffener will have a factor of safety of two against yielding.

3.3 Expanded Stiffener

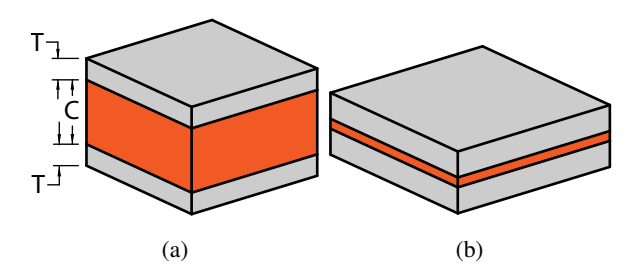


FIGURE 7: The dimensions associated with (a) the expanded stiffener and (b) its compressed state

A third option explored here for enhancing panel stiffness involves using an expanded stiffener as shown in Figure 7. In this device, the panel faces are made of a strong, dense material and the core (orange) is made of a low-density foam. This combination of materials has been shown to be very strong and stiff [25] compared to its weight and has been used widely in a variety of structures. However, the thickness of these sandwich structures can still be too large to effectively employ in origaminspired mechanisms because of the large number of layers that can be stacked in its folded form. This volume can be reduced if the foam core can be compressed elastically in the stowed state as shown in Figure 7b.

Two distinct cases of this method are described. In the first, it is assumed that the weight of the expanded stiffener must equal that of the panel being replaced. In this scenario, as the amount of foam in the stiffener is increased, the thickness of the walls will decrease. The second case will consist of a panel with walls that

are half the thickness of the original panel. This problem variation is considered because the panel walls may already be at a minimum thickness due to other constraints such as raw material dimensions. Consequently, the weight of this panel variation will increase as the amount of foam is increased. In both cases, the area moment of inertia gain as well as other important characteristics can be found.

For a foam-core sandwich panel with the dimensions shown in Figure 7a, the panel rigidity, EI, modulus of elasticity of the foam core, E_c , and panel mass, m, are given by [19]

$$EI = \frac{E_f b T^3}{6} + \frac{E_c b C^3}{12} + \frac{E_f b T (C+T)^2}{2}$$
 (18)

$$E_c = E_s \left(\frac{\rho_c}{\rho_s}\right)^2 \tag{19}$$

$$m = bCL\rho_c + 2bLT\rho_f \tag{20}$$

where b is the panel width, T is the thickness of the sandwich face, C is the thickness of the foam core, ρ_c is the density of the foam core, ρ_s is the density of the foam material, ρ_f is the density of the face material, E_f is the Young's Modulus of the face, E_c is the modulus of the foam core and E_s is the modulus of the core material. If we use Equation (19) to eliminate E_c in Equation (18) and make the substitution $\delta = \rho_c/\rho_s$, then the panel rigidity can be expressed as

$$EI = \frac{1}{12}bC^3\delta^2 E_s + \frac{1}{2}bC^2 E_f T + bC E_f T^2 + \frac{2}{3}bE_f T^3$$
 (21)

The area moment of inertia can be found if we compare the sandwich panel to another made solely of the face material. $E = E_f$ in this case and the area moment of inertia is

$$I = \frac{bC^3\delta^2 E_s}{12E_f} + \frac{1}{2}bC^2T + bCT^2 + \frac{2bT^3}{3}$$
 (22)

If the initial solid panel has a thickness of *t*, then its area moment of inertia is

$$I_0 = \frac{1}{12}bt^3 \tag{23}$$

However, before a gain R can be calculated, a relationship between T and t must be found. If the mass of the initial panel and the sandwich panel are equal, then we can use Equation (20) to write the following relationship and solve for t.

$$m(b,L,C,T)\big|_{C=0,T=t/2} = m(b,L,C,T)$$

$$t = \frac{C\delta\rho_s + 2T\rho_f}{\rho_f}$$
(24)

Dividing Equation (22) by Equation (23) and substituting Equation (24) to eliminate *t* yields

$$R_{a} = \frac{\rho_{f}^{3} \left(C^{3} E_{s} \rho_{c}^{2} + 2 E_{f} T \left(3 C^{2} + 6 C T + 4 T^{2} \right) \rho_{s}^{2} \right)}{E_{f} \rho_{s}^{2} \left(C \rho_{c} + 2 T \rho_{f} \right)^{3}}$$
(25)

$$=\frac{\eta^3 \left(8\lambda + \delta^2 q^3 + 6\lambda q^2 + 12\lambda q\right)}{\lambda (2\eta + \delta q)^3}$$
 (26)

if we make the parametric substitutions $\eta = \rho_f/\rho_s$, $\lambda = E_f/E_s$, $\delta = \rho_c/\rho_s$ and q = C/T.

A similar derivation and result can be obtained if we consider the case where a minimum panel thickness has already been reached. If this minimum face panel thickness is half the initial panel thickness t, then T = t/2 and the mass of this panel will be

$$m_w = bL \left(C\rho_c + t\rho_f \right) \tag{27}$$

The gain in area moment of inertia can be determined by making these substitutions and dividing by I_0 .

$$R_b = \frac{1}{8} \left(\frac{C^3 E_s \rho_c^2}{E_f T^3 \rho_s^2} + \frac{6C^2}{T^2} + \frac{12C}{T} + 8 \right)$$
 (28)

$$= \frac{1}{8} \left(\frac{\delta^2 q^3}{\lambda} + 6q^2 + 12q + 8 \right) \tag{29}$$

3.3.1 Collapse Behavior An important requirement for the expanded stiffener to function efficiently is for it to compress substantially and to use significantly less space when stowed. It must also be capable of undergoing this compression without requiring too much force. A minimal amount of collapse will diminish the potential benefits of implementing this system and requiring excessive force to compress the core may also cause problems for the storage and deployment mechanisms. These two constraints of core compression can be modeled and optimized to obtain a beneficial combination for a particular set of stiffener materials and design parameters.

The load required to collapse the core can be found through determining the collapse stress σ_{el} shown in Figure 8. When this stress is reached, open-cell foams will collapse with an approximately constant stress given by [26]

$$\frac{\sigma_{el}}{E_s} = 0.03\delta^2 (1 + \delta^{1/2})^2 \tag{30}$$

and will enter the densification region at a strain of [27]

$$\varepsilon_{cd} = 1 - \frac{\delta}{0.3} \tag{31}$$

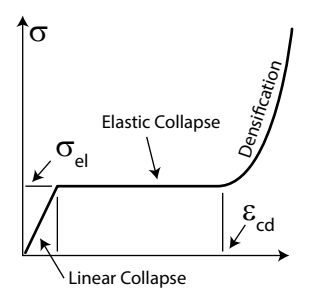


FIGURE 8: The stress-strain diagram of an elastic foam

Knowledge of this maximum collapse strain allows us to find *C* for the stowed panel:

$$C_{stowed} = (1 - \varepsilon_{cd})C = 3.33\delta C \tag{32}$$

4 Experimental Results

Confidence in the theoretical relations for two stiffener types was obtained through experiments and finite-element simulations. Because of the unique geometry of each stiffener type, multiple fixtures were needed. All finite element simulations were performed on models constructed with shell elements in ANSYS. Convergence studies were performed in each case to verify that convergence had occurred.

4.1 Partially-Actuated Stiffener

Testing the stiffness of a partially-actuated pattern was accomplished by constructing the prototype shown in Figure 9 using the fixture shown in Figure 10. Prototype dimensions are listed in Table 1. The material was sheet polypropylene and the panels adjacent to crease B were tilted to the θ value in the table. It was constructed with small Nylon hinges used for model aircraft stabilizers. The stiffness was measured by loading the vertex as a cantilevered beam in the fixture shown in Figure 10a. This fixture consisted of an upper (a) and lower (b) grip, two supporting columns (c) and a base (d) that can be secured to the workbench. The test specimen (1), Kistler 9212 load cell/deflector (2) and test fixture (3) are shown in Figure 10b.

Using the cantilever setup shown, three tests of a partially-actuated vertex were conducted. The actuation angle reported in Table 1 should result in an increase in stiffness of R=18.4 according to Equation 6. A similar value was found through an finite element simulations shown in Figure 11. The vertex was calculated to have a stiffness gain of R=15.0. An element size of 1.59 millimeters was used. The results from the tests of the actuated models showed that the stiffness increased by $R=15.8\pm3.8$. The confidence interval resulted from experiments on multiple samples. This differs by 16.9 % from the analytical results and 4.7% from the FEA result. Both results are

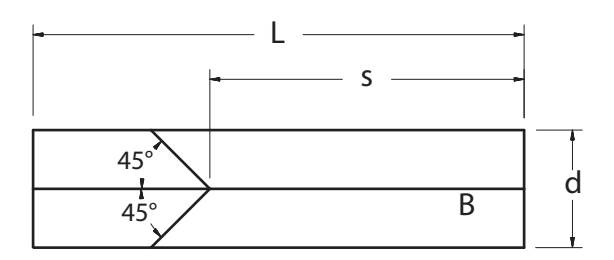
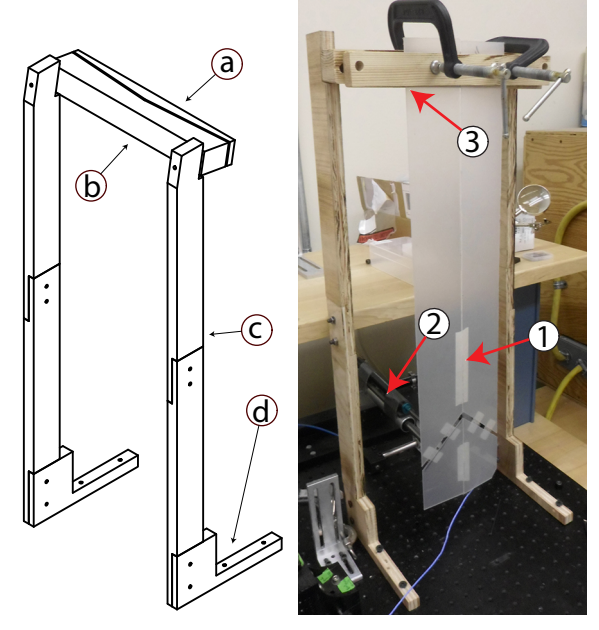


FIGURE 9: A fourth-order vertex that was partially actuated to demonstrate the resulting increase in stiffness



(a) A schematic of the test fix- (b) An image of the test setup

FIGURE 10: The test fixture used to measure the bending stiffness of an origami pattern

also within the 95% confidence intervals of the R value, which is reasonable considering the unmodeled flexibility of the frame, nonlinearity in the material properties, and other variables.

Other important assumptions made by the analysis include neglecting buckling in the panel. Such non-linear effects would alter the slight actuation angles and significantly alter the stiffness. Another assumption is that the hinges do not add significant amounts of flexibility. When this is not correct, parasitic motion at the hinges can alter the results.

This method can be attractive because the only requirement for it to function is that the pattern cannot completely unfold. Consequently, implementing it is relatively straightforward. A combination of appropriate hard-stops and self-locking hinges

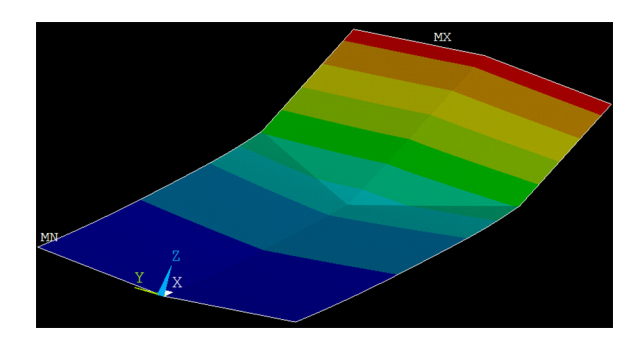


FIGURE 11: A finite-element simulation of a partially-actuated vertex

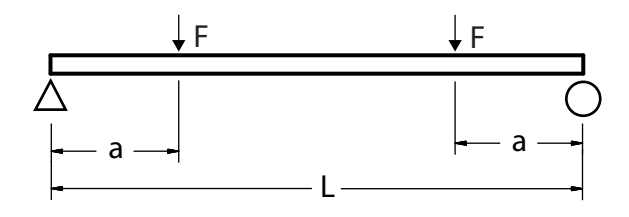


FIGURE 12: The parameters and loads applied during a four-point bend test

would be one method of ensuring the appropriate partially folded final state.

4.2 Yielded Stiffener

The predictions of stiffness increase for Equation (9) were confirmed experimentally using a four-point bend test illustrated in Figure 12.

The prototypes tested in this fixture were made of polypropylene sheets with properties shown in Table 2. For a four-point test shown in Figure 12, the deflection of the panel

TABLE 1: Parameters used to define the partially-actuated prototype

Parameter	Value	Units
E	1.5	GPa
ν	0.42	none
L	63.5	cm
S	40.6	cm
d	15.2	cm
t	0.159	cm
θ	0.0875	rad

is given by

$$y = \frac{Fx}{6EI}(x^2 + 3a^2 - 3La) \tag{33}$$

where F is the force load at one of the two load teeth, E is Young's Modulus, I is the area moment of inertia of the panel cross-section, x is the distance of a point from the outermost load point in the test and a is shown in Figure 12. Solving this equation for I where k = F/y and x = a yields

$$I = \frac{ka(4a^2 - 3La)}{6E}$$
 (34)

Using Equation (34), the mean stiffness gain for three samples was calculated to be $R_a=191\pm16$. The confidence interval resulted from experiments on multiple samples. This value compares favorably with the analytical prediction of $R_a=198$ from Equation (9). These results were supplemented by a finite-element simulation shown in Figure 13. The element size was 3.28 millimeters. This simulation predicted a gain of $R_a=232$. While there is an error of 17.0% between this value and the analytical results, this difference may result from the unmodeled effect of the crease used to deploy the stiffener. Any deviation of the stiffener from vertical during the loading process could also have influenced the results through a lateral torsional buckling mode. The analytical and experimental results agree closely and the FEA results are not widely different, building confidence in the model for the yielded stiffener.

5 Comparison of Stiffeners

One important question that arises about these methods is how they compare and what type of considerations will influence

TABLE 2: Parameters used to define the yielded stiffener prototype and test fixture

Parameter	Value	Units	
E	1.5	GPa	
v	0.42	none	
t	0.159	cm	
L	59.7	cm	
w	10.8	cm	
h	2.54	cm	
a	15.2	cm	

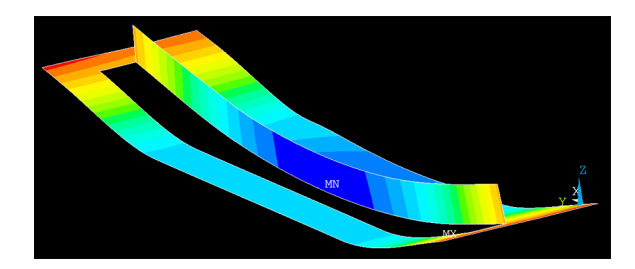


FIGURE 13: A finite-element simulation of the yielded stiffener

the selection of one method over another. Because the gain in the moment area of inertia for each stiffener depends on several parametric variables, a good comparison can only be made if a range of input values are considered. This can be done by graphing the moment of inertia gain, R, versus a certain cost variable P. Both R and P depend on the geometry and so are plotted parametrically.

One potential cost for each stiffener is the deployment ratio. Because each stiffener type either increases the volume of the panels or diminishes the available panel area, their use will decrease the final deployed area for a constant stored volume. Because many applications for deployable mechanisms seek to maximize deployed area, this may be an important design cost. For this comparison, the deployment ratio is defined as

$$\Delta_r = \frac{A_{deployed}}{V_{\text{stanged}}^{2/3}} \tag{35}$$

where $A_{deployed}$ is the area of a deployed pattern and V_{stowed} is the volume of the stored pattern. Because our objective is to compare stiffeners, the percent change in deployment ratio between a single, unit-square panel of thickness t and its stiffened counterpart will be defined as the area cost. The area cost can be written as

$$\Delta = \frac{\Delta_r - \Delta_r^s}{\Delta_r} = \frac{A_{deployed} - A_{deployed}^s}{A_{deployed}}$$
(36)

where Δ_r^s is the deployment ratio for the stiffened panel.

Another cost to consider is the increase in mass produced by each stiffener. This cost is represented by M and is defined as the percent change in panel mass between the stiffened and initial versions. Both the initial and final panels must have equivalent area.

5.1 Stiffener Area and Mass Costs

Before any effective comparison can be made, specific area costs described in Equation (36) must be found for all three stiffeners. For a partially-actuated pattern, its viewable area can be expressed as $A = A_0 \cos \theta$ where A_0 is the real panel area and θ

is the angle between the panel angle and a line from the base of the normal to the viewer. Because the stowed volume remains unchanged between stowed and deployed states, the area cost for partial actuation is given by

$$\Delta_{PA} = 1 - \cos \theta \tag{37}$$

Similar area costs can be found for the yielded and expanded stiffeners and are given by Equations (38) and (39).

$$\Delta_Y = \frac{h}{w} = f \tag{38}$$

$$\Delta_E = 1 - \frac{0.629961 \left(\frac{\delta q}{\eta} + 2\right)^{2/3}}{(1.665\delta q + 1)^{2/3}}$$
(39)

The result for the expanded stiffener was found after determining that the deployment ratios for the initial and stiffened version are

$$\Delta_r^0 = \frac{bL}{(bLt)^{2/3}} \tag{40}$$

and

$$\Delta_r^s = \frac{0.629961bL}{(bL(1.665C\delta + T))^{2/3}} \tag{41}$$

A similar set of mass costs can be found for the three stiffeners. Because the panels are constrained to have constant area, adding each stiffener will lead to increased mass. Partial actuation will diminish the viewable area and so more panel area will be required for increasing amounts of actuation. The yielded stiffener will also diminish panel area and so will requre larger panels and increased mass. Although the expanded stiffener does not reduce the area, the constant wall case will increase the mass through the addition of the core material.

For partial-actuation, the initial area A_0 required to achieve a constant viewable area A is given by $A = A_0 \cos \theta$. If we assume

TABLE 3: The equation number used for each parametric parameter (ξ), its cost variable (Δ or M) and stiffener type

	Δ	M	ξ
Partially-actuated	Eq. 6	Eq. 6	θ
Yielded stiffener	Eq. 9	Eq. 9	f
Expanded stiffener	Eq. 26	Eq. 29	q

that area is proportional to mass, then this relation can be used to determine the percent mass increase or mass cost for this design as

$$M_{PA} = \frac{m^s - m^0}{m^0} = \frac{1 - \cos \theta}{\cos \theta} \tag{42}$$

where M is the mass cost, m^s is the mass of a unit square panel with stiffeners and m^0 is the mass without.

For the yielded stiffener shown in Figure 4, the mass cost is

$$M_Y = \frac{h}{w} = f \tag{43}$$

The mass cost for the expanded stiffener can be found if we set the stiffened mass to Equation (20) where T=t/2 (half the initial panel thickness) and the initial mass is found when T=t/2 and C=0. Computing the mass cost as described previously gives

$$M_E = \frac{\delta q}{2\eta} \tag{44}$$

A comparison of these stiffeners can be made if we designate one variable in each equation as the independent variable ξ and make all other values constant. The variable chosen as ξ for each stiffener is shown in Table 3. This parametric variable ξ can then be used to generate plots of the functions $(R_a(\xi), \Delta(\xi))$ and $(R_b(\xi), M(\xi))$ for each stiffener. Plots of the stiffener area costs Δ versus their gain R are shown for the three stiffeners in Figure 14. A similar plot of their performance versus their mass cost is shown in Figure 15. In both plots, it can be seen that partial actuation demonstrates the largest increases in R for low costs in mass and area. Similarly, the expanded stiffener performance is the second best in both cases while the yielded stiffener is the most costly.

6 Conclusion

Managing the stiffness of an origami-inspired mechanism is an important capability to ensure that lightweight deployables can adequately fulfill their functions. In this paper, three types of deployable stiffeners to control pattern stiffness were investigated. Analytical equations modeling the increase in moment of inertia were derived for each stiffener type. The predictions of these equations were later verified experimentally and through finite-element simulations.

The equations expressing the increase in inertia were written parametrically with respect to a characteristic variable ξ and then plotted against two specific design costs. This enabled a comparison of their performance. This particular comparison showed that

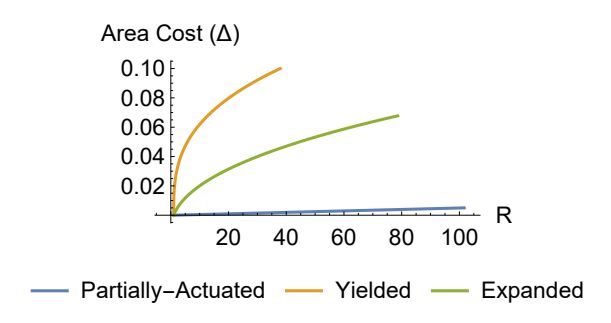


FIGURE 14: Plots of the parametric inertia gain $R(\xi)$ and $\Delta(\xi)$ with respect to the variable ξ .

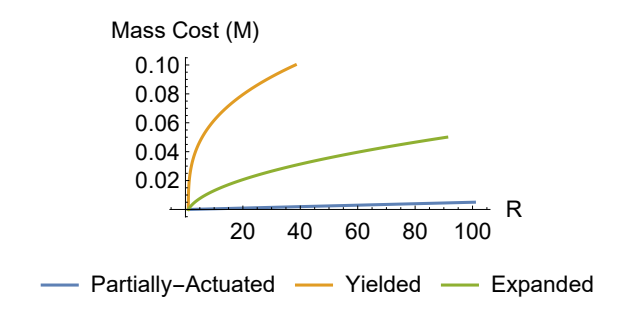


FIGURE 15: Plots of the parametric inertia gain $R(\xi)$ and $M(\xi)$ for the three stiffeners.

partial actuation is most efficient, followed by expanded stiffeners. While this comparison only considered three stiffener types and two costs, the method can be applied to other stiffeners and costs to facilitate design selection. It is hoped that this research will facilitate the design of origami-inspired deployables by providing the alternatives for designing stiff, deployed mechanisms.

Acknowledgement

This work was supported by a NASA Office of the Chief Technologist's Space Technology Research Fellowship and by the National Science Foundation and the Air Force Office of Scientific Research under NSF Grant EFRI-ODISSEI-1240417 and NSF Grant No. 1663345.

REFERENCES

- [1] Kuribayashi, K., Tsuchiya, K., You, Z., Tomus, D., Umemoto, M., Ito, T., and Sasaki, M., 2006. "Self-deployable origami stent grafts as a biomedical application of ni-rich tini shape memory alloy foil". *Materials Science and Engineering: A*, **419**(12), pp. 131 137.
- [2] Thrall, A., and Quaglia, C., 2014. "Accordion shelters: A historical review of origami-like deployable shelters de-

- veloped by the US military". *Engineering Structures*, **59**, pp. 686 692.
- [3] Ario, I., Nakazawa, M., Tanaka, Y., Tanikura, I., and Ono, S., 2013. "Development of a prototype deployable bridge based on origami skill". *Automation in Construction*, **32**, pp. 104 111.
- [4] Saintsing, C. D., Cook, B. S., and Tentzeris, M. M., 2014. "An origami inspired reconfigurable spiral antenna". In ASME 2014 International Design Engineering Technical Conferences, Vol. 5B, p. V05BT08A050.
- [5] Reynolds, W. D., Jeon, S. K., Banik, J. A., and Murphey, T. W., 2013. "Advanced folding approaches for deployable spacecraft payloads". In International Design Engineering Technical Conferences, Vol. 6B, p. V06BT07A043.
- [6] Zirbel, S. A., Lang, R. J., Thomson, M. W., Sigel, D. A., Walkemeyer, P. E., Trease, B. P., Magleby, S. P., and Howell, L. L., 2013. "Accommodating thickness in origamibased deployable arrays". *Journal of Mechanical Design*, 135(11), p. 111005.
- [7] Higuchi, K., and Ishimura, K., 2009. "A survey of space structures research in Japan". In 50th AIAA/ASME/ASCE/AHS/ASC Structures, Structural Dynamics, and Materials Conference. American Institute of Aeronautics and Astronautics, May.
- [8] Hedgepeth, J. M., 1982. "Accuracy potentials for large space antenna reflectors with passive structure". *Journal of Spacecraft and Rockets*, **19**(3), May, pp. 211–217.
- [9] Masterson, R. A., Miller, D. W., and Grogan, R. L., 2002. "Development and validation of reaction wheel distrubance models". *Journal of Sound and Vibration*, 249(3), pp. 575– 598.
- [10] Ross, R. G., 2003. "Vibration suppression of advanced space cryocoolers: an overview". In Smart Structures and Materials 2003: Damping and Isolation, Vol. 5052, pp. 5052 12.
- [11] Takahshi, T., Nakamoto, N., Ohtsuka, M., Aoki, T., Konishi, Y., and Yajima, M., 2009. "A simple on-board calibration method and its accuracy for mechanical distortions of satellite phased array antennas". In 3rd European Conference on Antennas and Propagation, pp. 1573 1577.
- [12] Yellowhorse, A., and Howell, L. L., 2018. "Deployable lenticular stiffeners for origami-inspired mechanisms". *Mechanics Based Design of Structures and Machines*, pp. 1–16.
- [13] Lee, T.-U., and Gattas, J. M., 2016. "Geometric design and construction of structurally stabilized accordion shelters". *Journal of Mechanisms and Robotics*, **8**(3), March, pp. 031009–8.
- [14] Klett, Y., Middendorf, P., Sobek, W., Haase, W., and Heidingsfeld, M., 2017. "Potential of origami-based shell elements as next-generation envelope components". In 2017 IEEE International Conference on Advanced Intelli-

- gent Mechatronics (AIM), pp. 916-920.
- [15] Tan, L. T., and Pellegrino, S., 2006. "Thin-shell deployable reflectors with collapsible stiffeners part 1: approach". *AIAA Journal*, **44**(11), pp. 2515–2523.
- [16] Jorgensen, J., Louis, E., Hinkle, J., Silver, M., Zuckermandel, B., and Enger, S., 2005. "Dynamics of an elastically deployable solar array: Ground test model validation". In 46th AIAA/ASME/ASCE/AHS/ASC Structures, Structural Dynamics and Materials Conference. American Institute of Aeronautics and Astronautics, April.
- [17] Schenk, M., and Guest, S. D., 2011. *Origami 5*. Taylor & Francis Inc, ch. Origami Folding: A Structural Engineering Approach, pp. 291–304.
- [18] Filipov, E. T., Tachi, T., and Paulino, G. H., 2015. "Origami tubes assembled into stiff, yet reconfigurable structures and metamaterials". *Proceedings of the National Academy of Sciences*, **112**(40), pp. 12321–12326.
- [19] Cheung, K. C., Tachi, T., Calisch, S., and Miura, K., 2014. "Origami interleaved tube cellular materials". *Smart Mater. Struct.*, **23**(9), p. 094012.
- [20] Wonoto, N., Baerlecken, D., Gentry, R., and Swarts, M., 2013. "Parametric design and structural analysis of deployable origami tessellation". *Computer-Aided Design and Applications*, **10**(6), pp. 939 951.
- [21] Evans, T. A., Lang, R. J., Magleby, S. P., and Howell, L. L., 2015. "Rigidly foldable origami gadgets and tessellations". *R. Soc. Open Sci.*, **2**(9), p. 150067.
- [22] Liu, Y., Genzer, J., and Dickey, M. D., 2016. "2D or not 2D: Shape-programming polymer sheets". *Progress in Polymer Science*, **52**, pp. 79 106.
- [23] Overvelde, J. T., de Jong, T. A., Shevchenko, Y., Becerra, S. A., Whitesides, G. M., Weaver, J. C., Hoberman, C., and Bertoldi, K., 2016. "A three-dimensional actuated origamiinspired transformable metamaterial with multiple degrees of freedom". *Nature Communications*, 7(10929).
- [24] Shigley, J. E., 2011. *Shigley's Mechanical Engineering Design*. Tata McGraw-Hill Education.
- [25] Vinson, J. R., 2001. "Sandwich structures". *Appl. Mech. Rev*, **54**(3), May, pp. 201–214.
- [26] Gibson, L. J., and Ashby, M. F., 1988. *Cellular solids: structure and properties*. Pergamon Press.
- [27] Li, Q. M., Magkiriadis, I., and Harrigan, J. J., 2006. "Compressive strain at the onset of densification of cellular solids". *Journal of Cellular Plastics*, **42**(5), September, pp. 371–392.